Available online at www.sciencedirect.com
SCIENCE DIRECT®
Progress in Oceanography 69 (2006) 218–238
Progress in Oceanography
www.elsevier.com/locate/pocean

Eddies and Tropical Instability Waves in the eastern tropical Pacific: A review

Cynthia S. Willett [a,*], Robert R. Leben [a], Miguel F. Lavín [b]

[a] Department of Aerospace Engineering, CCAR, University of Colorado, Boulder, CO 80309-0431, USA
[b] Department of Physical Oceanography, CICESE, Ensenada, Mexico

Abstract

Mesoscale eddies and tropical instability waves in the eastern tropical Pacific, first revealed by satellite infrared imagery, play an important role in the dynamics and biology of the region, and in the transfer of mass, energy, heat, and biological constituents from the shelf to the deep ocean and across the equatorial currents.

From boreal late autumn to early spring, four to 18 cyclonic or anticyclonic eddies are formed off the coastal region between southern Mexico and Panama. The anticyclonic gyres, which tend to be larger and last longer than the cyclonic ones, are the best studied: they typically are ~180–500 km in diameter, depress the pycnocline from ~60 to 145 m at the eddy center, have swirl speeds in excess of 1 m s^{-1}, migrate west at velocities ranging from 11 to 19 cm s^{-1} (with a slight southward component), and maintain a height signature of up to 30 cm. The primary generating agents for these eddies are the strong, intermittent wind jets that blow across the isthmus of Tehuantepec in Mexico, the lake district in Nicaragua and Costa Rica, and the Panama canal. Other proposed eddy-generating mechanisms are the conservation of vorticity as the North Equatorial Counter Current (NECC) turns north on reaching America, and the instability of coastally trapped waves/currents.

Tropical Instability Waves (TIWs) are perturbations in the SST fronts on either side of the equatorial cold tongue. They produce SST variations on the order of 1–2 °C, have periods of 20–40 days, wavelengths of 1000–2000 km, phase speeds of around 0.5 m s^{-1} and propagate westward both north and south of the Equator. The Tropical Instability Vortices (TIVs) are a train of westward-propagating anticyclonic eddies associated with the TIWs. They exhibit eddy currents exceeding 1.3 m s^{-1}, a westward phase propagation speed between 30 and 40 km d^{-1}, a signature above the pycnocline, and eastward energy propagation. Like the TIWs, they result from the latitudinal barotropically unstable shear between the South Equatorial Current (SEC) and the NECC with a potential secondary source of energy from baroclinic instability of the vertical shear with the Equatorial Undercurrent (EUC).

This review of mesoscale processes is part of a comprehensive review of the oceanography of the eastern tropical Pacific Ocean.

Keywords: Mesoscale eddies; Eddy dynamics; Tropical instability waves; Tropical oceanography; Eastern tropical Pacific

* Corresponding author. Tel.: +1 215 489 4030.
E-mail address: cwillett@colorado.edu (C.S. Willett).

0079-6611/$ - see front matter © 2006 Elsevier Ltd. All rights reserved.
doi:10.1016/j.pocean.2006.03.010

1. Introduction

The advent of satellite oceanography in the 1970s revealed the ubiquity of the so-called mesoscale phenomena (gyres, eddies, jets, fronts, meanders). This discovery triggered observational and modeling efforts that have shown the mesoscale to be a very important component of dynamical oceanography at all scales (e.g. in transporting momentum, heat, mass, energy, chemical and biological properties). In the eastern and central tropical Pacific, important mesoscale phenomena include the eddies that originate off the coast of Central America and southern Mexico (Fig. 1), and the Tropical Instability Waves (TIWs), with their associated eddies, that are found on the zonal borders of the equatorial cold tongue (Fig. 2). We shall here use the names "coastal eddies" and Tropical Instability Vortices (TIVs) for the former and latter type of eddies, respectively. The Costa Rica Dome, not covered here, is an integral part of the mean and seasonal hydrography, circulation

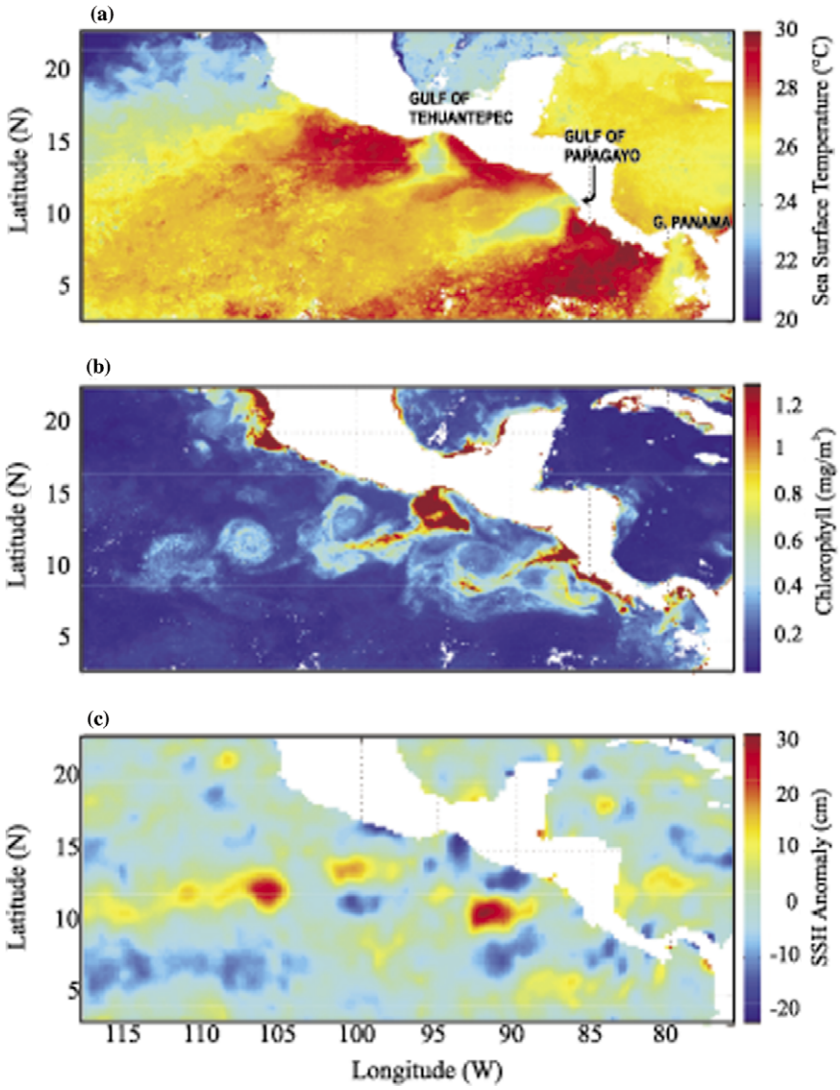

Fig. 1. Signatures of eddies generated near the Gulfs of Tehuantepec and Papagayo are seen in (a) sea surface temperature, (b) chlorophyll concentration, and (c) sea surface height anomaly. The SST and color images are 8-day composites (10–18 February 2004) from the MODIS instrument on board the Aqua satellite (http://oceancolor.gsfc.nasa.gov). The near real-time sea surface height anomaly is from February 14, 2004 (http://ccar.Colorado.edu/realtime).

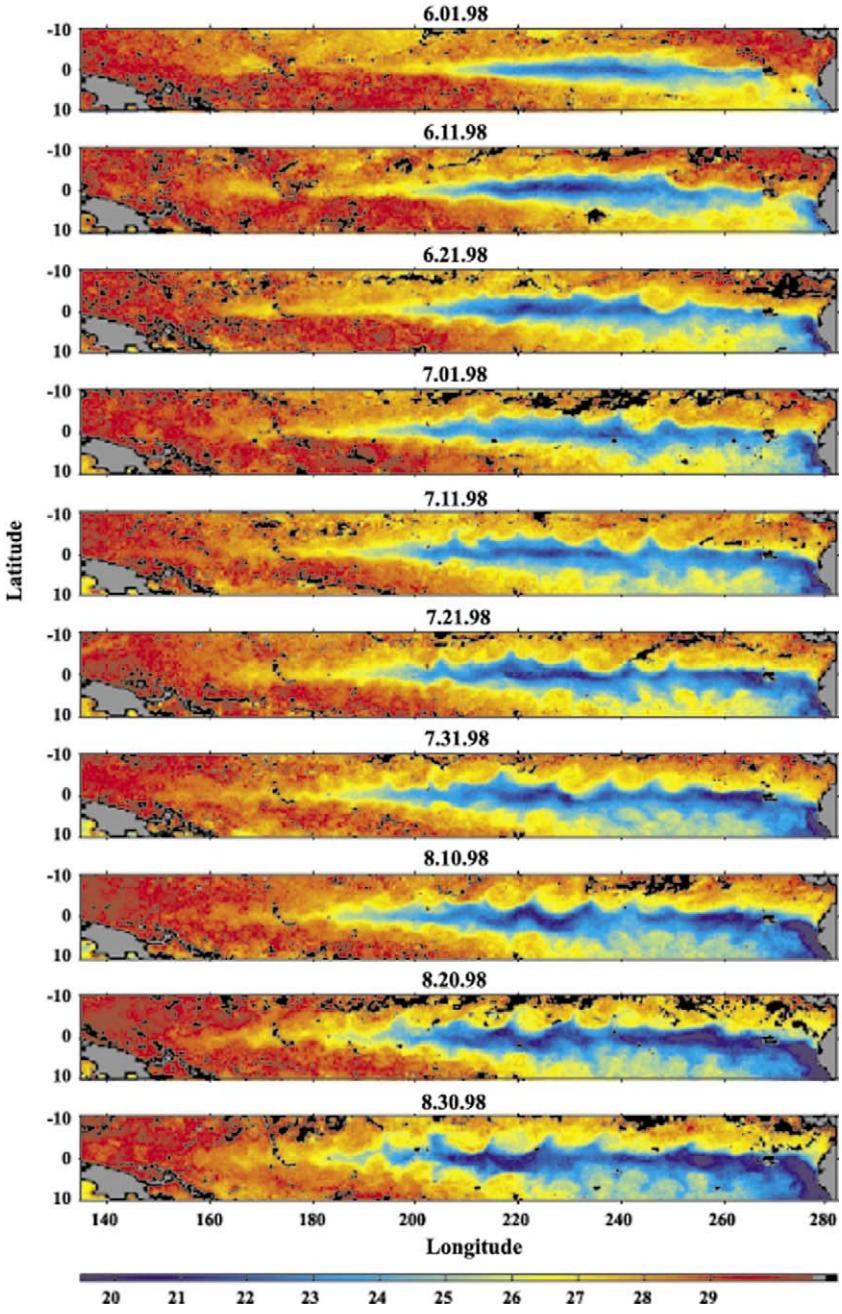

Fig. 2. Tropical instability waves (TIW) seen in imagery from the Tropical Rainfall Measuring Mission (TRMM) Microwave Imager (TMI). TMI imagery courtesy of Remote Sensing Systems (http://www.ssmi.com/).

and biology of the eastern tropical Pacific (Fiedler, 2002; Kessler, 2002). Thus, it is covered in the respective chapters of this review (Fiedler and Talley, 2006; Kessler, 2006; Fernández-Alamo and Farber-Lorda, 2006).

The purpose of this article is to summarize our present knowledge about these mesoscale phenomena and their importance in the oceanography of the eastern tropical Pacific. The generation, characteristics, and life histories of these processes are closely linked to patterns in the atmosphere (Amador et al., 2006), to local hydrography (Fiedler and Talley, 2006), and to the ocean circulation in the region (Kessler, 2006). The impact of these phenomena on the surrounding ecosystem (Müller-Karger and Fuentes-Yaco, 2000; Samuelsen, 2005) is briefly addressed.

2. Coastal eddies

2.1. History

Stumpf (1975) and Stumpf and Legeckis (1977) published the first satellite thermal infrared images of eddies generated in the Gulf of Tehuantepec and near the Gulf of Papagayo. They were the first to show that these eddies were anticyclonic and made the first estimates of their westward propagation speed. They also proposed that the eddies were generated by the trans-isthmic wind jets of the Gulf of Tehuantepec, which had previously been described by Hurd (1929). Roden (1961) studied the jet's effect on the SST and large-scale dynamics of the gulf.

This initial detection of the coastal eddies by satellite imagery was followed a decade later by a series of modeling efforts (Clarke, 1988; McCreary et al., 1989; Umatani and Yamagata, 1991) that unraveled the basic physics, and by the first direct observations of their thermohaline structure and currents in the Gulf of Tehuantepec (Barton et al., 1993; Trasviña et al., 1995). While direct observations of these eddies remain scarce, satellite oceanography has continued to provide more and better tools for their study. In addition to the continued availability of thermal images (AVHRR), there is now a large (and increasing) amount of information about height (TOPEX/POSEIDON), color (CZCS, SeaWiFS, MODIS), and winds (NSCAT, QuikScat). These sensors have been used to study the eddies and a good portion of the information presented here has been gained through them. Analytical and numerical modeling have also contributed important knowledge. Now very powerful eddy-resolving numerical simulations are available through the Internet using Naval Research Laboratory (NRL) Layered Ocean Models (NLOM).

The different satellite sensors have contributed to the description of different evolutionary stages eddies, as determined by the eddies' characteristics, the surrounding ocean, and the meteorology of the area. The high intensity of the trans-isthmic wind jets produces vertical mixing in the surface layers of the sea, which lowers the sea surface temperature (SST) and enhances local chlorophyll production, thus providing two satellite-detectable tracers for the study of the generation stage of the eddies.

Early descriptions were somewhat vague about the relative roles of mixing and Ekman pumping in lowering the SST. Perhaps the ambiguity was because the condition of a wind jet blowing perpendicular to the coast was new and the term "upwelling" had a well established meaning as "coastal upwelling" due to Ekman pumping close to the coast by along-shore winds. It is now known that the strikingly low SST patches that occur offshore right under the wind maximum are caused by vertical mixing in the strongly stratified surface layers typical of the area, and not by Ekman pumping (upwelling) (Roden, 1961; Clarke, 1988; Barton et al., 1993; Trasviña et al., 1995). Vertical mixing can be due to direct stirring and by shear instability; Trasviña et al. (1995) calculated the gradient Richardson number from observed profiles of temperature and currents to show that shear instability was occurring only during the wind event. In order to avoid confusion, we will use "Ekman pumping" instead of "upwelling" for the situation away from the coastal zone. Evidence for upwelling very close to the coast is present in some satellite images (e.g. Fig. 2b of Barton et al., 1993), but the cool patches are much smaller than those offshore and are shorter lived.

Although the warming of the shallow ocean surface layer masks the eddies' surface temperature signature within days of the wind abating, satellite radiometer data have been used by Clarke (1988), McCreary et al. (1989), Barton et al. (1993), Trasviña et al. (1995), Müller-Karger and Fuentes-Yaco (2000), and Ballestero and Coen (2004) to produce a detailed description of the eddies during the generation process. Synthetic Aperture Radar images have also been used to describe wind and circulation features during this stage (Martinez-Diaz-de-Leon et al., 1999). The color signature of the eddies is longer-lived than the sea surface temperature signal, which has allowed their tracking for up to four months (Müller-Karger and Fuentes-Yaco, 2000; McClain et al., 2002; Gonzalez-Silvera et al., 2004); thus providing information about their westward path and translation speed.

The phytoplankton concentrations within the eddies vary from less than $0.25\,mg\,m^{-3}$ to more than $10\,mg\,m^{-3}$ depending on eddy age, generation time, and spin direction. The positive chlorophyll anomalies indicate that these eddies are important mechanisms in transporting organisms and nutrients away from the coastal boundary of the eastern tropical Pacific (Müller-Karger and Fuentes-Yaco, 2000). This is analogous with the Gulf Stream rings, but quantitative estimates based on in situ observations are still lacking. Mül-

ler-Karger and Fuentes-Yaco (2000) claim that chlorophyll carried by these eddies results initially from coastal upwelling and is later maintained by processes within the eddies. They found low (high) phytoplankton concentrations in the eddies generated between late April and October (November and early April). Although this seems reasonable for cyclones, it is unclear what processes maintain the positive chlorophyll anomaly in the longer-lived anticyclonic eddies.

The surface height anomalies intrinsic to the dynamics of the eddies (up to ±30 cm, "lows" for cyclonic or cold-core eddies, "highs" for anticyclonic or warm-core eddies) are detectable in the sea surface height (SSH, Fig. 1c) measurements from radar altimeters (Hansen and Maul, 1991; Giese et al., 1994; Willett, 1996). Altimeters measure SSH along the satellite ground track; so multiple satellite passes have to be combined to map the eddy field. As a result, satellite altimeter data do not have as fine a spatial resolution as that of the scanning radiometers. Also, the temporal sampling from exact repeat orbits (10–35 days) causes the altimeter to miss detection of short-lived eddies. The studies by Müller-Karger and Fuentes-Yaco (2000) and by Gonzalez-Silvera et al. (2004) include many short-lived eddies that would be missed by altimetric sampling. However, since radar altimeters are not affected by clouds, altimetry allows the continuous monitoring of the evolution of the large-diameter and long-lived eddies. Because eddies maintain a height signature until dissipation, their entire lifespan can be accurately monitored using radar altimetry.

2.2. Generation

Since the detection of the coastal eddies in the Gulfs of Tehuantepec and Papagayo, their generation was linked to the trans-isthmic wind jets (described by Amador et al., 2006, and briefly in Section 2.2.1), and to Ekman pumping. Models that simulated the peculiar condition of a narrow jet blowing offshore normal to the coast were developed in the early eighties (Crepon and Richez, 1982). The basic physics of the proposed gyre generation is Ekman pumping associated with the wind stress curl. This pumping is asymmetric with respect to the wind jet axis and produces horizontal Ekman transport convergence (downward Ekman pumping) on the right side of the jet and divergence (upward Ekman pumping) on the left (looking downwind in the northern hemisphere).

However, the wind-generates-eddy scenario does not explain every eddy observed in the eastern tropical Pacific (Hansen and Maul, 1991; Müller-Karger and Fuentes-Yaco, 2000; Brenes et al., 1988) and numerical models have generated them without wind forcing (Umatani and Yamagata, 1991; Zamudio et al., 2001). Alternative generation mechanisms that have been proposed (reviewed in Section 2.2.2) are the conservation of potential vorticity as the NECC is deflected north by the coast to become the Costa Rica Coastal Current (CRCC) (Hansen and Maul, 1991), and instabilities of the CRCC (Zamudio et al., 2001).

2.2.1. Generation by trans-isthmic wind jets

The intense wind bursts, collectively called Nortes (here we call them "trans-isthmic wind jets"), are involved in the generation of the coastal eddies, and are channeled through three gaps in the Sierra Madre mountain range: The Tehuantepec Jet across the Isthmus of Tehuantepec, the Papagayo Jet over the central lowlands of Nicaragua, and the Panama Jet across the Isthmus of Panama (see map in Fiedler and Lavín, 2006). Fig. 3 from Chelton et al. (2004) shows the four-year averages (August 1999–July 2003) of the spatial high-pass filtered curl of the wind stress (Fig. 3a) and of the SST and vector-average wind stress (Fig. 3b).

The Tehuantepec jets are due to high surface atmospheric pressure over the Gulf of Mexico caused by winter storms passing across North America behind cold fronts that penetrate to 18° N and occasionally to 12° N. If the high atmospheric pressure penetrates far enough south, Papagayo and Panama jets will be generated. However, the wind jets over Papagayo and Panama are usually driven by trade wind variations, tropical storms, and tropical cyclones, and are usually unrelated to Tehuantepec bursts (Chelton et al., 2000b).

The wind jets occur most frequently from October through February, but conditions for an individual event may occur at any time of the year (Chelton et al., 2000a,b; Romero-Centeno et al., 2003). The jets are intermittent, occurring every few weeks and lasting from one to several days, with mean speeds $\sim$20 m s^{-1} and maxima up to 30 m s^{-1}. As the wind leaves the coast, it spreads out and turns right, potentially following an inertial path, with a radius $\sim$300 km. The inertial circle is not completed because of friction and other processes (Clarke, 1988; Steenburgh et al., 1998; Bourassa et al., 1999; Chelton et al., 2000a,b, 2004).

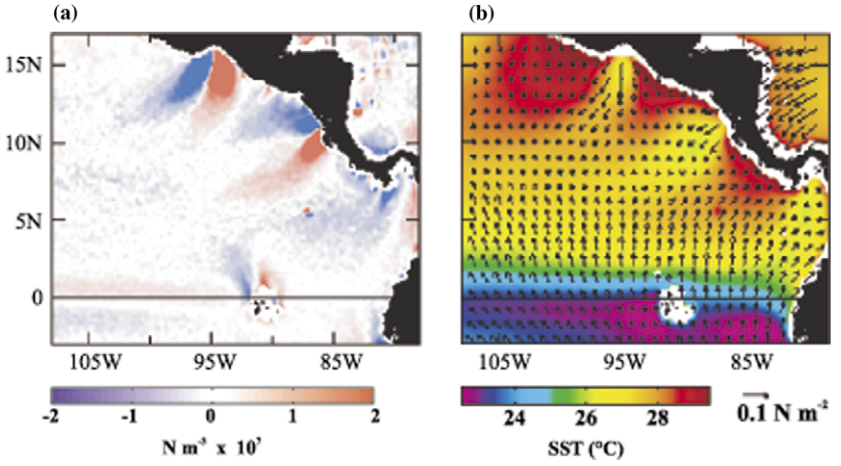

Fig. 3. Four-year averages (August 1999–July 2003) of: (a) the spatially high-pass filtered curl of the wind stress, and (b) the SST and vector-average wind stress. From Chelton et al. (2004). Courtesy of Dr. D. Chelton.

The basic physics involved in the eddy generation by the trans-isthmic jets is sketched in Fig. 4, based on the 11/2-layer linear baroclinic ocean model of Clarke (1988); we are looking downwind, and the section is well away from the coast. The wind stress $\boldsymbol{\tau} = (\tau_x, 0)$ along the x-axis (into the page) generates in the upper layer of the ocean an Ekman transport to its right given by $V_E = -\tau_x/\rho f$, which varies along the y-axis depending on the functional form of $\tau_x(y)$, as suggested by the arrows pointing in the $-y$ direction. The inhomogeneous $V_E(y)$ causes current convergence (divergence) to the right (left) of the wind, which by continuity produces Ekman pumping with vertical velocity

$$w_E = (\rho f)^{-1} \text{ curl } \boldsymbol{\tau} = -(\rho f)^{-1} \mathrm{d}\tau_x/\mathrm{d}y,$$

which is downward (upward) on the right (left) side of the jet. On the convergence (divergence) side, the pycnocline is depressed (lifted) by a few tens of meters, while the sea surface rises (falls) by a couple of

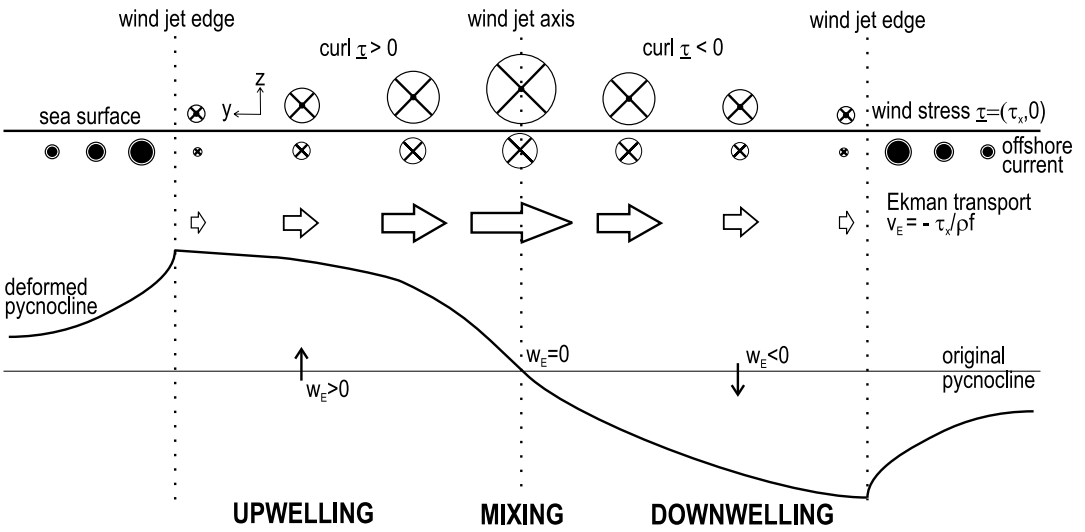

Fig. 4. Sketch of the basic baroclinic model of eddy generation by trans-isthmic jets by Ekman pumping, inspired by the model of Clarke (1988). We are looking offshore along the x-axis, and the section is well away from the coast. No scales are given. The magnitude of the wind stress along the x-axis (into the page) is represented by the diameter of the circumscribed X symbol above the sea surface. Ekman transport in the upper layer is represented by the arrows pointing to the right. The offshore velocity (into the page) in the upper layer is represented by the diameter of the circumscribed X symbol and the onshore velocity (out of the page) by that of the filled circles.

decimeters. The surface topography is a squashed mirror image of the pycnocline distortion; it is not shown in the diagram because of its small magnitude, but it is detectable by satellite scatterometers.

The distortion of the density field sets up pressure gradients, which when balanced by Coriolis force, produce in the upper layer a geostrophic flow in the $+x$ direction under the wind jet and in the $-x$ direction beyond it (Fig. 4), decaying in y with the scale of the Rossby radius of deformation. Roden (1961) carried the analysis this far, and noticed that the thermocline in the Gulf of Tehuantepec reported by Blackburn (1962, then in manuscript) was depressed to the west of the jet and lifted to the east.

There are several mechanisms proposed for the next step, which is generation of the eddies. Clarke (1988) noticed that the eddies were of approximately the same scale as the natural Rossby radius of deformation of the wind jet, and proposed that inertial deflection of the wind jet and resultant Ekman transport toward the center of the inertial radius could spin-up anticyclonic eddies (as if a sketch similar to Fig. 4, but with all signs changed, were attached to the left edge of the wind jet). In support, he argued that the largest and strongest eddies were anticyclonic, and that the offshore patches of low SST were elongated and curved anticyclonically, marking the jet path. However, it is now known from numerical models and satellite scatterometer estimates of the wind stress that although the Tehuantepec wind jet does turn to its right, the inertial circle is not completed because the jet fans out, becomes geostrophic, and can be affected by local and large-scale conditions (Steenburgh et al., 1998; Bourassa et al., 1999; Chelton et al., 2002a, 2002b).

McCreary et al. (1989) used 11/2-layer analytical and numerical models forced by a sustained wind jet of finite offshore extent, falling in intensity as cosines (across, offshore and in time). Linear and non-linear models were used, and vertical entrainment could be included to simulate vertical mixing in a simplified way. They find that while the jet is strengthening, an ageostrophic offshore flow produces upwelling at the coast and lowers the underlying sea level; as the wind abates, the flow is reversed. If entrainment is not included, the model generates an anticyclonic eddy to the right (looking offshore) of the wind jet and a cyclonic one to its left. When entrainment is included, low SST patches appear under and to the left of the jet, while the cyclonic eddy is eliminated because mixing weakens the uplifted thermocline that maintains it. Thus, their model with entrainment predicted predominantly warm core anticyclonic eddies. However, the wind speed used by McCreary et al. (1989), sustained at $\sim$45 m s^{-1}, is unrealistically high which leaves open the question of the reason for the predominance of anticyclonic eddies.

An alternative explanation for the lack, or weakness, of cyclonic eddies during generation by offshore wind jets, proposed by Thomas and Rhines (2002), considers the non-linearities induced by Ekman pumping and advection, by causing vortex stretching, secondary circulation, and heat flux. When other flows are present or generated during the spin-up process (secondary circulation, geostrophic currents in both layers), the Ekman transport is $V_E = -\tau_x/\rho(f+\zeta)$, where $\zeta = \partial v/\partial x - \partial u/\partial y$ is the vertical component of the relative vorticity, so that the Ekman pumping velocity is more complicated:

$$w_E = [\rho(f+\zeta)]^{-1}\partial\tau_x/\partial y - \tau_x\rho^{-1}[(f+\zeta)]^{-2}\partial\zeta/\partial y.$$

ζ is part of the expression of potential vorticity, $q = (\zeta + f)/h$, which is a conservative property in the absence of forcing, and that stems directly from the equations of motion (e.g., Cushman-Roisin, 1994, pp. 57–58; also see Kessler, 2006). Thomas and Rhines (2002) show that Ekman transport is enhanced (reduced) in zones of anticyclonic (cyclonic) vorticity, which enhances downward pumping to the right of the wind (reduces upward pumping on its left). Another non-linear aspect that has the same effect, at least during the initial stages, is related to the vertical and horizontal advection of the momentum of the flow in the Ekman layer. By considering the non-linear aspects of the heat flows in the process, they also find that horizontal temperature gradients are enhanced in the downwelling region and weakened in the upwelling regions; this thermodynamic process also makes anticyclonic vorticity stronger than cyclonic vorticity.

Barton et al. (1993) suggest that the anticyclonic eddies may be generated by a series of wind events, rather than by a single one. Müller-Karger and Fuentes-Yaco (2000) mention that in their series of satellite data, cyclonic eddies seemed most likely to form when a shorter burst of strong winds was followed by a quiescent period of low-intensity winds. Neither of these hypotheses has been further investigated.

2.2.2. Generation by vorticity conservation and instability of coastal currents

The strong eastward flow of the NECC in autumn-winter (see Fig. 7 of Kessler, 2006) is forced to turn poleward by the American coast, which increases the planetary vorticity (f). So for potential vorticity (q) to be conserved (assuming no changes in stratification) the relative vorticity (ζ) has to decrease; in other words anticyclonic vorticity must be acquired. Hansen and Maul (1991) show that a modelled ring at 12° N (with the characteristics observed by them) had a q_{eddy} smaller than the climatological ambient potential vorticity at that latitude; the anomaly was equivalent to the increase of f between the latitude of the NECC and that of the eddy. Hansen and Maul (1991) also propose that boundary friction in the Costa Rica Coastal Current (CRCC) could be a secondary source of anticyclonic vorticity.

Although Hansen and Maul (1991) offer no details of the eddy formation process, instability of the CRCC is suggested. The argument of instability of the CRCC as a mechanism for generating eddies was recently analyzed by Zamudio et al. (2001). They use a numerical ocean model (Naval Research Laboratory Layered Ocean Model) and sea surface height altimeter observations (TOPEX/POSEIDON and ERS-2) to investigate the formation of eddies off the coast of Mexico. A poleward coastal jet with strong vertical shear is hypothesized to develop during strong El Niño events when downwelling Kelvin waves interact with the CRCC. The strengthening shear flow increases the amplitude of oscillations in the CRCC, which breaks into cyclonic and anticyclonic eddies. Although Zamudio et al. (2001) analyze an ENSO case, the coast of Central America and Mexico are influenced interannually and intraseasonally by poleward propagating disturbances originated in the equatorial zone (Enfield and Allen, 1983; Spillane et al., 1987; Kessler and McPhaden, 1995), which could induce similar instabilities in the CRCC, and eddy formation.

Observations suggesting the presence of anticyclonic eddies off the coast of Central America when transisthmic jets are not present lend support to the instability hypothesis of eddy formation. The occasional presence of eddies in satellite images obtained during the boreal summer is reported by Müller-Karger and Fuentes-Yaco (2000), and surface temperature and salinity patterns off Central America presented by Brenes et al. (1988) strongly suggest that they may be part of the climatology.

The relative importance of these mechanisms for eddy formation in this region is still unclear, but it is likely that all of them play some role in the process, with the wind jets being most prominent between November and March.

2.3. Characteristics

Four to 18 solitary eddies, anticyclonic or cyclonic, have been reported to form yearly in the coastal region during boreal autumn, winter, and spring (Willett, 1996; Müller-Karger and Fuentes-Yaco, 2000; Gonzalez-Silvera et al., 2004). Anticyclonic eddies are more numerous, larger, and last longer than cyclonic eddies. Willett (1996) find an average of 5.3 anticyclonic eddies formed per year, with a larger number during El Niño. After formation, eddies propagate west-southwest to about 120° W between 10° N and 15° N. They typically have a 90–250 km radius, they exhibit translation velocities from 11 to 19 m s^{-1}, have a height signature of up to 30 cm, and relatively high kinetic energy of 2.9×10^{15} J (Hansen and Maul, 1991). Direct current measurements with moored current meters and underway Acoustic Doppler Current Profilers (ADCP) have reported swirl velocities over 1.0 m s^{-1} (McCreary et al., 1989; Barton et al., 1993; Trasviña et al., 1995). Similar speeds are reported from satellite-tracked drifters (Hansen and Maul, 1991; Trasviña et al., 2003; Ballestero and Coen, 2004) and from altimetry (Willett, 1996). These eddies tend to increase in diameter and elongate zonally with time (Willett, 1996; Müller-Karger and Fuentes-Yaco, 2000).

In contrast to the many satellite-data studies, there appears to be only one comprehensive observational study of these eddies, and it was done in January 1989 in the Gulf of Tehuantepec. Physical aspects were reported by Barton et al. (1993) and Trasviña et al. (1995, 2003), and biological aspects by Robles-Jarero and Lara-Lara (1993), Farber-Lorda et al., 1994, and Farber-Lorda et al. (2004). They report the evolution of the coastal ocean before and after a moderate wind event. Even before the wind event the thermocline was depressed to the west and lifted to the east, but the wind event enhanced the pattern and made it visible in the satellite SST images. Within one day of the start of the wind event, the SST fell by up to 10 °C in an offshore-elongated patch that curved cyclonically. The lowest temperature, under the wind jet, was bounded by SST fronts; the western side was the strongest. The SST fronts developed meanders, suggesting instabilities,

and showed eastward advection of warm water along the coast. The anticyclonic eddy shown in Fig. 5a appeared to evolve from these features (Barton et al., 1993; Trasviña et al., 1995, 2003).

The subsurface temperature and salinity distributions and the currents measured with the ADCP are described in detail by Barton et al. (1993) and Trasviña et al. (1995, 2003). The eddy was symmetrical, had a diameter of ~250 km; the pycnocline was depressed to ~120 m in the center, and the eddy had azimuthal velocities over 1 m s^{-1}. In contrast, on the eastern side of the Gulf, the thermocline was squashed just below the 30 m-thick surface mixed layer where the currents were weak (~0.2 m s^{-1}) and northward. Fig. 5 shows a hydrography section across the Gulf of Tehuantepec (marked in blue in Fig. 1a) that cuts the eddy close to its northern edge; the distributions of temperature and salinity show the lifting to the surface to form fronts, and the geostrophic velocity suggests that countercurrents were present near the eddy edge.

Direct observations of the thermohaline structure of anticyclonic eddies after they have traveled west from the formation area are reported by Willett (1996) and Trasviña et al. (2003). Hansen and Maul (1991) show an XBT section plus a few CTD casts. An example of subsurface temperature and salinity sections of a mature anticyclonic eddy from the eastern tropical Pacific is shown in Fig. 6. The CTD data were collected on a WOCE cruise that was traveling north along 110° W in April 1994. The regional hydrography (Fiedler and Talley, 2006) has an average thermocline depth around 50 m, which rises towards the Central American coast, and deepens north of 15° N; salinity increases slightly poleward throughout the water column. The depression in the thermocline (Fig. 6), centered at 13° N is an anticyclonic eddy with a diameter of 500 km, estimated from altimeter data (Willett, 1996). The eddy core is ~125 m thick, fresher than the ambient waters north of the eddy (Fig. 6). The geostrophic velocity shows cyclonic circulation between 9° N and 16° N, with the eastward flow (~0.2 m s^{-1}) slower than the westward flow (~0.35 m s^{-1}), most likely because the eddy is immersed in the westward North Equatorial Current. The thermocline displacement corresponds with anomalies of other tracer properties including salinity, oxygen, nutrients, Freon, and helium/tritium (Willett, 1996).

The still older eastern tropical Pacific eddy observed by Hansen and Maul (1991) also had an estimated diameter approaching 500 km and azimuthal current speeds of 1 m s^{-1}. Using altimetry they found a local sea surface height anomaly of ~35 cm, a depressed pycnocline to 145 m (from XBT data), and a salinity slightly lower than the surroundings.

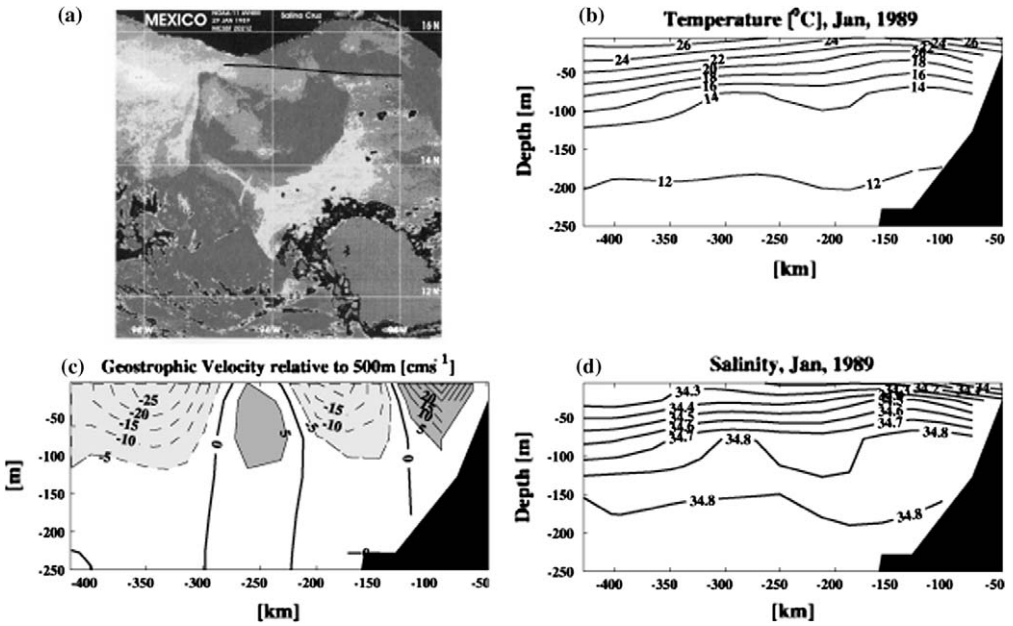

Fig. 5. Structure of Tehuantepec eddy formed in January 1998. (a) Sea surface temperature on January 30, 1998. Vertical structure below the blue line is shown, after smoothing by objective analysis: (b) potential temperature (°C); (c) geostrophic velocity (cm s^{-1}) relative to 500 m, negative values mean flow out of the page; (d) salinity (psu).

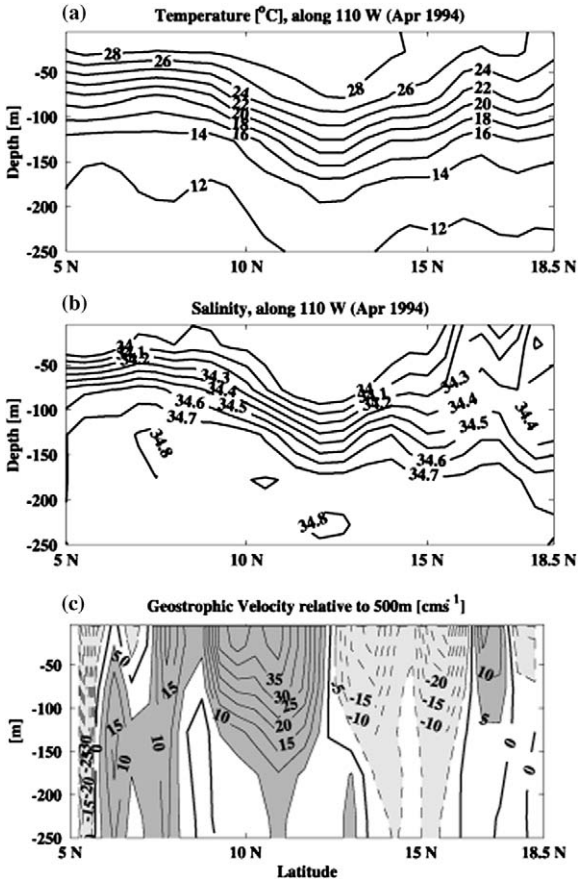

Fig. 6. Hydrograpy and geostropic velocity sections along 110° W, from 5 to 18.5° N. CTD data were collected on the R/V Discoverer WOCE cruise during April of 1994. Only the top 250 m are shown. (a) Potential temperature (°C), (b) salinity, (c) geostrophic velocity (cm s^{-1}, negative velocity means eastward flow), relative to 1000 m. Smoothing with objective analysis (cutoff scales 100 km in the horizontal, 70 m in the vertical) was performed on the temperature and salinity distributions before calculating the geostrophic current.

2.4. Propagation

Once eddies are formed, their behavior is described by appropriate versions of the equations of motion. In particular, they are observed to propagate westward, a behavior that from the early observations was understood to be due to the β effect (explained below). A southward drift is also detected in the anticyclonic eddies. In order to give some physical insight into the reason for the eddies' observed behavior and the meaning of the differences between the calculated and observed translation speeds, we make a short description of the physics of eddies in the ocean, based on Cushman-Roisin (1994). The names of variables to be used are shown in the schematic cyclonic and anticyclonic baroclinic eddies in Fig. 7. The discussion in this section will consider only the northern hemisphere situation ($f > 0$).

In an ocean rotating with frequency $f/2$, parcels of water moving in the absence of forces (inertial motion) will describe an anticyclonic circle whose radius (inertial radius) depends on f and on the speed $U(R_I = U/f)$, while the period of rotation (inertial period) depends only on f: $T_I = 2\pi/f$. If a wave or perturbation moves with speed c, the distance traveled during an inertial period is $cT_I = 2\pi(c/f) = 2\pi R_d$. The ratio $R_d = c/f$ is called the Rossby radius of deformation, one of the most important characteristics of oceanic flows since it gives a length scale above which the effects of the Earth rotation must be taken into account. The behavior and properties of an eddy depend on its size relative to the radius of deformation.

For a simply stratified ocean like that shown in Fig. 7, with one upper layer of density ρ_s over a deep layer of density ρ_d, internal waves (interface perturbations) move with speed $c = \sqrt{(g'h)}$, where $g' = g(\rho_d - \rho_s)/$

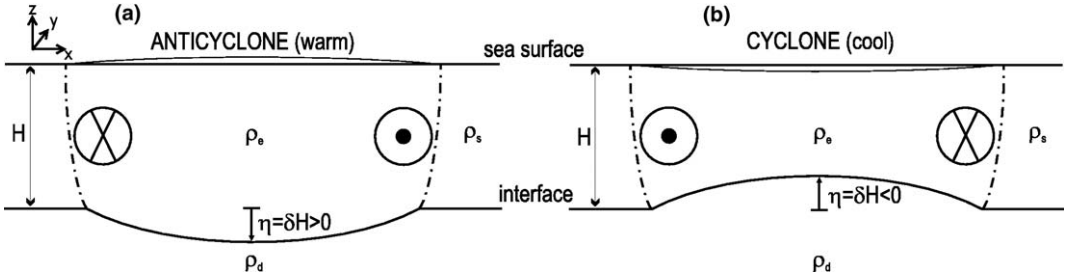

Fig. 7. Schematic surface eddies: (a) anticyclonic, (b) cyclonic. δH is the interface distortion from horizontal, positive downward. Densities: ρ_e = density inside the eddy, ρ_s = surface density of the surroundings, ρ_d = density of the deep layer.

$\rho_0 = g\Delta\rho/\rho_0$ is the reduced gravity (ρ_0 is a reference density) and h is the depth of the surface layer. The corresponding Rossby radius, which includes the effect of stratification, is called the internal or baroclinic radius of deformation $R_{\text{int}} = \sqrt{(g'h)}/f = O(50\text{ km})$. Henceforth it is understood that R_d and the names "radius of deformation" or "Rossby radius" refer to R_{int}. Estimates of R_d for the eddy generation zones are 70 km for Tehuantepec, 90 km for Papagayo, and 150 km for Panama (Chelton et al., 1998).

In the absence of forcing, the equations are:

$$\frac{\partial u}{\partial t} + u\frac{\partial u}{\partial x} + v\frac{\partial u}{\partial y} - (f_0 + \beta_0 y)v = -\rho_0^{-1}\frac{\partial p'}{\partial x} = -g'\frac{\partial \eta}{\partial x},$$

$$\frac{\partial v}{\partial t} + u\frac{\partial v}{\partial x} + v\frac{\partial v}{\partial y} + (f_0 + \beta_0 y)u = -\rho_0^{-1}\frac{\partial p'}{\partial y} = -g'\frac{\partial \eta}{\partial y},$$

$$\frac{\partial \eta}{\partial t} + \frac{\partial (hu)}{\partial x} + \frac{\partial (hv)}{\partial y} = 0,$$

where the pressure anomaly compared with the surroundings is $p' = \rho_0 g'\eta$, where η is the deformation of the interface (Fig. 7). The variation of the Coriolis parameter with latitude $f = f_0 + \beta_0 y$ (y is positive northward), where $\beta_0 = [\mathrm{d}f/\mathrm{d}y]_0$, is included because some eastern Pacific eddies can extend by a few degrees in latitude. Here f_0 and β_0 are the value of the parameters in the central latitude ($y = 0$) of the process under study.

The Coriolis force term is so important in these equations that the relevance of the other terms is measured against it. In particular, the relative importance of the advective non-linear terms is measured by the Rossby number

$$Ro = u(\partial u/\partial x)/fu = U/\Omega L,$$

where we have substituted the variables for their typical scales: $[u] = U$, $[x] = L$, $[f] = \Omega$, the square brackets mean "scale of", and Ω is the Earth's rotation rate ($7.29 \times 10^{-5}\ \mathrm{s}^{-1}$). If Ro is much less than unity, the motion is linear; the closer to unity the more non-linear the motion. For the anticyclonic eastern Pacific eddies, Hansen and Maul (1991) calculated the Rossby number as swirl speed divided by the product of the meridional radius, r_m, and the Coriolis parameter, f_0. They found Ro ranges from 0.13 to 0.22, which means that they are non-linear.

The steady-state solution of the linear version of the equations of motion is the geostrophic balance, and some of the wave-like solutions when f can be taken as constant (the f-plane) are the inertial motion, and Kelvin and Poincaré waves. In this approximation, the physics of eddies is best understood in cylindrical coordinates, with r measured from the center of the eddy and v (the orbital velocity) positive counterclockwise. The balance of forces in the radial direction is

$$-v^2/r - fv = -\rho_0^{-1}\partial p/\partial r$$

where $p(r)$ is the pressure distribution inside the eddy, due to the interface distortion (Cushman-Roisin, 1994). If there is no pressure gradient, inertial motion is obtained. It is a non-linear equation because of the centrifugal force (v^2/r), and in this case $Ro = U/fL$, where L is the scale of the eddy radius. If the pressure difference is

due to a surface lens (Fig. 8) with density anomaly $\Delta\rho$ and thickness h compared with the ambient fluid, $[\partial p/\partial r] = \Delta P/L = \Delta\rho g h/L = \rho_0 g' h/L$, as before.

If only the linear terms are considered (very small Ro), the geostrophic balance results: $U = \Delta P/\rho_0 fL = g'\eta/fL$. Thus, $Ro = U/fL = (R_d/L)^2$: a small Ro occurs for scales large compared to R_d, so that "large eddy" means $L \gg R_d$. In other words, the linearity of an eddy can be determined by comparing its radius against R_d. Eddies much larger than the radius of deformation are linear and therefore geostrophic.

In the "large" eddies the centrifugal force is smaller than the Coriolis and the pressure forces. The analysis is valid for cyclonic or anticyclonic eddies. For the centrifugal force to be of the same order as Coriolis force (Ro of order unity which means non-linear), $1 \approx U/fL = \sqrt{(g'h)}/fL = R_d/L$; that is, the radius of the eddy has to be of the same scale as the radius of deformation ($L \sim R_d$). These are eddies of "intermediate size", and the non-linearity affects cyclones and anticyclones differently: for a given radius and pressure anomaly, the orbital velocity is faster in anticyclones than in cyclones. In anticyclones (cyclones) the centrifugal force acts in the same (opposite) direction as the pressure force, which requires an increased (reduced) velocity for the Coriolis force to achieve balance. The coastally generated eddies of the eastern tropical Pacific are intermediate to large. This is because for the Tehuantepec eddy generation area, the eddy radii are ~125–250 km, or only $\sim 2R_d$, while the oldest and largest anticyclonic eddies (with a radius ~250 km) are $\sim 3.5R_d$.

The case $Ro \gg 1$ means that Coriolis force is negligible compared with the centrifugal force. The balance of forces is between the pressure force and the centrifugal force (cyclostrophic balance); thus only low-pressure eddies are possible, but they can rotate clockwise or counterclockwise. If the motion is not geostrophic, it is occurring within time scales shorter than the inertial period, and therefore with a spatial scale or radius (L) smaller than the radius of deformation; in other words, eddies with radius smaller than R_d are cyclostrophic.

When the motion takes place over meridional distances such that the changes in f are important, the β terms must be used. The linear equations (large R_0) in the β-plane have Fourier-type solutions $[\cos(lx + my - \omega t)]$ provided that the frequency and the wave (ω) numbers (l,m) satisfy:

$$\omega = -\beta_0 R_d^2 \frac{l}{1 + R_d^2(l^2 + m^2)}.$$

The dispersive waves that satisfy this dispersion relation are called linear Rossby waves (or linear planetary waves), and their frequency is smaller than f. If their wavelength L ($=1/m \sim 1/l$) is shorter than or similar to R_d, the frequency is $\omega \approx \beta_0 L \ll f$, while if L is larger than R_d, $\omega \approx \beta_0 R_d^2/L \approx \beta_0 L \ll f$. While the meridional wave speed ($c_y = \omega/m$) can be northward or southward, the zonal wave speed is always westward:

$$c_x = \frac{\omega}{l} = \frac{-\beta_0 R_d^2}{1 + R_d^2(l^2 + m^2)}.$$

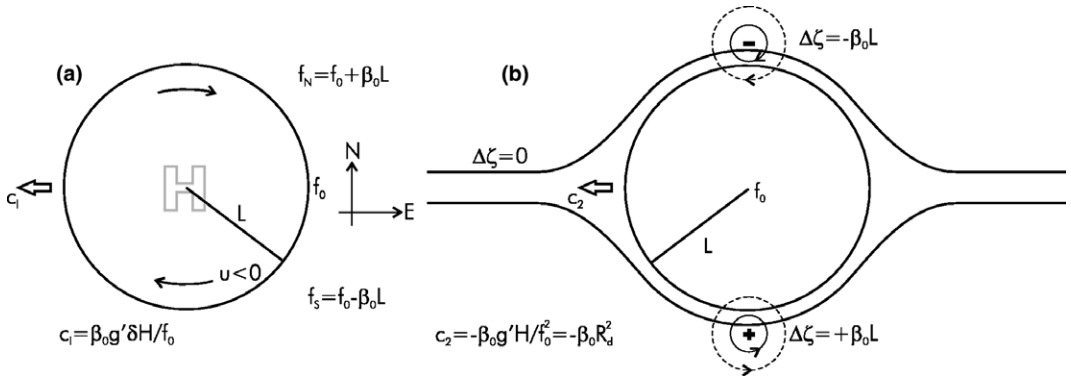

Fig. 8. Eddy drift mechanisms. (a) Self advection by parcels inside the eddy, due to difference in f in the northern and southern sides of the eddy; anticyclones drift westward (illustrated), and cyclones eastward. (b) Westward propulsion as a Rossby wave by potential vorticity conservation of fluid displaced by the passage of the eddy (after Cushman-Roisin et al., 1990).

If the waves are very long (wavelengths much larger than R_d), the waves become non-dispersive and propagate strictly westward, at the maximum speed allowed, which is $c_{max} = -\beta_0 R_d^2$. This value is used as a benchmark by comparing it against the westward drift of observed or modeled eddies. Estimated values for c_{max} are: 11 cm s^{-1} for Tehuantepec, 18 cm s^{-1} for Papagayo, 51 cm s^{-1} for Panama. Also important are that linear Rossby waves cannot have a frequency higher than $\beta_0 R_d/2$ and that the group velocity, which is the speed at which wave energy travels, of long (short) Rossby waves is westward (eastward).

If the process is such that the non-linear terms must be included, as in the eastern Pacific eddies, the mathematics become more involved, and numerical models have to be used, like those of Umatani and Yamagata (1991) and McCreary et al. (1989). The latter authors, in addition to modeling the formation of eddies by a wind jet, also observed that their westward migration was slightly faster than c_{max}, which they found to be due to the non-linear terms.

Cushman-Roisin et al. (1990) classify mesoscale ocean eddies into (a) quasi-geostrophic eddies of the open ocean ($L \approx R_d$, $\delta H \ll H$), where δH is the scale of η (Fig. 8) and (b) frontal-geostrophic rings in the vicinity of western-boundary currents ($L > 3R_d$,$\delta H \approx H$). They mention that generally Ro and the beta number ($\beta = \beta_0 L/f_0$) are small, therefore the eddies are non-linear and are primarily in geostrophic balance. As a consequence their swirl time-scale is much larger than the inertial period. For the coastal eddies of the eastern tropical Pacific, Hansen and Maul (1991) estimate $Ro \approx 0.13$–0.22, while above we estimated $L \approx 2$–$3R_d$. The pycnocline depression is large, similar to the thermocline depth in the area: $\delta H \approx H \approx 70$ m (Hansen and Maul, 1991; Barton et al., 1993; Trasviña et al., 1995, 2003); therefore they are non-linear and more like frontal-geostrophic rings. Observation-based estimates of the ageostrophic velocity in a Tehuantepec eddy (Trasviña et al., 2003) show values $\sim$0.3 m s^{-1}.

One approach for estimating eddy properties is to specify an initial structure (radius, density difference, velocity distribution), and then leaving it to evolve on its own, or to estimate potential and kinetic energy. The westward translation of baroclinic eddies has been studied this way by Nof (1983) and others (see Cushman-Roisin et al. (1990) for more references), and by Hansen and Maul (1991) and Willett (1996) for the tropical Pacific eddies. For the westward migration, an approach has been to obtain the equations of the center of mass of the eddies, and Cushman-Roisin et al. (1990) propose a very general expression for the translation speed of near-geostrophic eddies:

$$\frac{dX}{dt} = -\frac{\beta_0 g'}{f_0^2} \frac{\int\int (H\eta + \eta^2/2) dx dy}{\int\int \eta dx dy}, \quad \frac{dY}{dt} = 0,$$

where the local layer thickness h is the sum of the mean layer thickness (H) and a local interface displacement η ($h = H + \eta \geqslant 0$), with $[\eta] = \delta H$. Since the two double integrals have the same sign, all eddies in near-geostrophic balance drift westward ($dX/dt < 0$). From the formula it can be proved that for very weak eddies ($\eta \ll H$, or quasi-geostrophic), the drift speed is constant at $-\beta_0 R_d^2$, the same as that of the long non-dispersive Rossby waves (c_{max}). It is the same for cyclonic or anticyclonic eddies.

For eddies in which η is a substantial fraction of H (like the Gulf Stream rings and the eastern Pacific eddies), it is possible to obtain bounds for the drift speed. From the formula above: for anticyclones, η is positive, the terms in the numerator are added and the drift is faster than c_{max}. The larger the interface displacement, the faster the eddy. However, the speed cannot exceed $\beta_0 g'(H + h_{max})/2f_0^2$, where h_{max} is the maximum interfacial depth at the center of the eddy. For cyclones, η is negative, and therefore the drift speed cannot exceed c_{max}. The larger the interface displacement, the slower the drift. Since the interface distortion is limited by the depth of the surface layer, the minimum drift speed for anticyclones is $c_{max}/2$.

A physical explanation for the westward migration of baroclinic eddies is given by Cushman-Roisin et al. (1990). There are two distinct mechanisms involved, the most important being the reaction upon the eddy from the ambient fluid displaced as the eddy passes through it (Fig. 8, right panel); the perturbation moves westward as a Rossby wave. The zonal motion is initiated by a weaker mechanism, which is induced by the imbalance of the Coriolis force on the particles swirling inside the eddy (Fig. 8, left panel). The two mechanisms are included in the formula

$$c = -\frac{\beta_0 g' \delta H}{f_0^2} - \frac{\beta_0 g' H}{f_0^2} = -\frac{\beta_0 g' \delta H}{f_0^2} - \beta_0 R_d^2.$$

The first term gives eastward drift for cyclones ($\delta H < 0$) and westward for anticyclones ($\delta H > 0$). However, the second term dominates because $H > \delta H$; therefore all near-geostrophic eddies move westward, but the cyclones are slower than the anticyclones.

Measurements of the westward migration speed of anticyclonic coastal eddies are: Stumpf and Legeckis (1977) $\sim$14.2 cm s^{-1}, Hansen and Maul (1991) $\sim$15 cm s^{-1}, Barton et al. (1993) $\sim$11.6 cm s^{-1}, and Giese et al. (1994) $\sim$17 cm s^{-1}. Most estimates are in excess of the wave speed of a linear Rossby wave, which may be due to the second term in the equation above. In the model of McCreary et al. (1989) it is due to the non-linear terms associated with an increased layer thickness at the center of the eddies and with the divergence of momentum flux.

Note that the meridional movement in the formulae above is zero. Barotropic eddies have been shown to have an additional north–south movement, equatorward for anticyclonic and poleward for cyclonic (Adem, 1956; Firing and Beardsley, 1976; Matsuura and Yamagata, 1982). The baroclinic eddies in the model of Umatani and Yamagata (1991) move southwestward. Cushman-Roisin (1994) proposes a qualitative mechanism that would work during the early formation of the eddies, making cyclones drift north and anticyclones south; in both cases the meridional drift causes (through q conservation) a reduction of the eddy's relative vorticity, which means a spin-down of the eddy. At the moment, the observed southward component of the coastal eddies of the eastern tropical Pacific does not have a satisfactory explanation.

2.5. Dissipation

An altimetry study of the anticyclonic coastal eddies (Willett, 1996) shows that they can survive for up to six months, traveling up to 3000 km from the generation area. The Tehuantepec eddies seem to be the longest lived, followed in longevity by the Papagayo eddies. The Panama eddies are quite short-lived, existing at most for about 14 days (Willett, 1996; Müller-Karger and Fuentes-Yaco, 2000), and dissipating before reaching 85° W. It has been proposed that this is due to the interaction of the eddies with the Guardian Bank (Hansen and Maul, 1991), a bottom topographic feature extending west-southwest from the coast of Costa Rica with a width of about 100 km (Fig. 1 of McClain et al., 2002).

Compared with other eddies of similar size, even the life-span of Tehuantepec eddies is relatively short, which Hansen and Maul (1991) suggest is attributable to the relatively small available potential energy (APE) content of the eddies, estimated as $\sim 4.1 \times 10^{15}$ J, which in turn is due to a relatively large regional radius of deformation. In this respect, the eastern tropical Pacific eddies are considered weak when compared to Loop Current eddies (an APE of 15×10^{15} J) or Agulhas Current eddies (an APE of 41×10^{15} J). Slow frictional dissipation of eddy kinetic energy is another factor in the decay of eddies. Hansen and Maul (1991) also proposed that the slight southward drift of these eddies may bring them into contact with the NECC, where they would be eliminated; this possibility has not yet been analyzed. The spin-down of these eddies by Rossby wave radiation has also not been investigated.

2.6. Cyclonic eddies

Although cyclonic eddies are visible in SST and color satellite images, and they seem to be more numerous than originally thought (Müller-Karger and Fuentes-Yaco, 2000; Gonzalez-Silvera et al., 2004), they have been less studied than the anticyclonic. Apparently a few large cyclonic eddies are generated each year and most are short-lived. While direct observations and numerical models agree that vertical mixing inhibits their formation by the trans-isthmic jets, it is unclear how they are formed. Under certain conditions they could be formed by Ekman pumping; however, it is more likely that they form by frontal instabilities becoming jets and anvil-shapes. Barton et al. (1993) suggest that cyclonic eddies may be generated as instabilities in the periphery of the anticyclonic eddies, and Gonzalez-Silvera et al. (2004) report the same. Some of the cyclonic eddies reported by Müller-Karger and Fuentes-Yaco (2000) and Gonzalez-Silvera et al. (2004) have radii less than R_d. More systematic study of the cyclonic eddies is necessary.

2.7. Effects on ecosystems

The biological-enriching effect of the wind burst events that give rise to the eastern tropical Pacific eddies is well documented, both from direct observations and through satellite color images (Pennington et al., 2006; Fernández-Alamo and Farber-Lorda, 2006). The Gulfs of Tehuantepec, Papagayo and Panama stand out as fertile zones in the infertile warm water pool of the eastern Pacific. The chlorophyll-rich areas associated with these gulfs extend up to 1000 km offshore, and it is generally assumed that these extensions are mostly due to the coastal eddies. Eddies can entrain and trap nutrients and organic material during the formation stage, and carry them offshore when they propagate westward (Fig. 1a). The initial ageostrophic surface current under the wind jets can also produce offshore transport.

The biological production processes have been simulated numerically by Samuelsen (2005), based on a hydrodynamic model with data assimilation. She finds that although there is offshore flux most of the year in the Gulf of Tehuantepec, the largest offshore volume flux and offshore transport of organic material occur during the eddy-generation periods. Müller-Karger and Fuentes-Yaco (2000) claim that chlorophyll carried by the eddies results initially from coastal upwelling and is later maintained by (unspecified) processes within the eddies. Although this seems reasonable for cyclones (which have upwelling in the center), it is unclear what processes maintain the positive chlorophyll anomaly in the longer-lived anticyclonic eddies. Their findings of low (high) phytoplankton concentrations in the eddies generated between late April and October (November and early April) agree with the primary productivity analyses of Pennington et al. (2006) and with the numerical model of Samuelsen (2005).

3. Tropical Instability Waves and Tropical Instability Vortices

Tropical Instability Waves (TIWs) and associated anticyclonic Tropical Instability Vortices (TIVs) are significant in near surface momentum and heat balances (oceanic and atmospheric) across the entire tropical Pacific. They occur mostly west of the ETP (Fig. 2); therefore, they will be reviewed here less thoroughly than the coastal eddies.

TIWs (Fig. 2), are westward-traveling perturbations in the SST fronts on either side of the equatorial cold tongue, which is centered near 1° S and east of 140° W (Contreras, 2002; Fiedler and Talley, 2006). They occur in both the Atlantic and the Pacific oceans. Although we highlight here the Pacific TIWs, reference is also made to findings in the Atlantic because the phenomena are basically the same. Differences arise because of the different extent of the basins, shape of the continental boundaries, features of the equatorial current systems, and position of the ITCZ. For recent articles with reviews of the Atlantic TIWs and TIVs, see e.g. Jochum et al. (2004) or Caltabiano et al. (2005).

3.1. History

The discovery of TIWs almost 30 years ago in current meter records in the Atlantic by Duing et al. (1975) and in infrared satellite images of the Pacific by Legeckis (1977) has led to extensive research by remote sensing, historical data, theoretical analysis, numerical modeling and direct observation with moored instruments, ships and drifters. Arrays of instrumented moorings have been maintained for decades in the equatorial Pacific (TOGA/TAO), and recently in the Atlantic (PIRATA), which has provided long records for analysis. Studies based on satellite data are quite numerous in recent years because of the wide range of important variables being measured routinely. Specific studies have also been conducted, for example, the Tropical Instability Wave Experiment (TIWE) in the Pacific in 1990 (Qiao and Weisberg, 1995, 1998), in which detailed observations of a TIV were made (Flament et al., 1996; Kennan and Flament, 2000). Similar observations were made in the Atlantic by Menkès et al. (2003). These intense investigations, which began immediately after the first detection of TIWs, have been maintained since these phenomena occur within a few degrees of the equator, a zone of enormous importance for the global climate.

After initial discovery of TIWs, Legeckis et al. (1983) reported the persistent appearance of the cusp-shaped wave patterns along equatorial SST fronts during the boreal summer months every year (from 1975 to 1983), except the two strong El Niño years (1976 and 1982). Philander (1976, 1978) hypothesized that a barotropic

instability arising from the shear between the NECC and the SEC causes these undulations in the Pacific. Cox (1980) supports this theory with a multilevel numerical model, and contributes important secondary hypotheses of the creation of eddy energy from baroclinic instability of the vertical shear and the conversion of mean potential energy to eddy energy. Hansen and Paul (1984) support the primary and secondary theories, and add estimates of eddy energy exchange and equator/poleward heat transport in the near-surface waters. Qiao and Weisberg (1995, 1998) stress the importance of the Equatorial Undercurrent in wave energetics from the TIWE, and provide an excellent summary of the work done on TIWs and TIVs from 1976 to 1992. Studies since then have looked at heat budget analysis (Kessler et al., 1998; Swenson and Hansen, 1999; Jayne and Marotzke, 2002), the interaction with the atmospheric boundary layer (Baturin and Niiler, 1997; Polito et al., 2001; Chelton et al., 2001; Benestad et al., 2001; Hashizume et al., 2002), association with the ENSO cycle (Yu and Liu, 2003), and the influence of Rossby waves (Lawrence and Angell, 2000). More direct observations are planned for the near future, with emphasis on the impact of TIVs on ecosystems and the interaction of the TIW with the marine boundary layer.

3.2. Generation

It is known that the TIWs are generated by instability processes associated with the intense velocity shear between the westward SEC and the eastward EUC and NECC (Philander, 1978; Contreras, 2002); although there is still some controversy regarding the relative importance of the NECC-SEC and EUC-SEC shears (Chelton et al., 2003). Qiao and Weisberg (1998) used moored ADCP data to suggest that TIWs are generated by barotropic instability from the cyclonic shear between the SEC and the Equatorial Undercurrent just north of the equator; they also found that local barotropic production continued to maintain and modulate the TIWs subsequent to generation. Numerical model results by Masina et al. (1999) suggest that TIWs grow from both barotropic and baroclinic conversions of energy. Their energy analysis indicated that baroclinic instability dominated the generating mechanism along the northern temperature front, and that eddy pressure fluxes radiated energy south of the equator.

The TIVs are a train of westward propagating anticyclonic eddies intimately associated with the TIWs (Legeckis, 1977; Hansen and Maul, 1991; Flament et al., 1996; Weidman et al., 1999; Kennan and Flament, 2000). Like the TIWs, they result from the latitudinal barotropically unstable shear between the SEC and the NECC (Philander, 1978), with a potential secondary source of energy from baroclinic instability of the vertical shear and the conversion of potential energy to eddy kinetic energy (Cox, 1980). Weidman et al. (1999) found them to be consistently generated 1.0° to the north of the local position of the wave front. Although the TIVs appear in the images as phase-locked with TIW undulations, the observations of a Pacific TIV by Flament et al. (1996) and Kennan and Flament (2000) show that they are distinct from the TIWs, as described below.

3.3. Characteristics

The TIWs are characterized by undulations in the north and south SST fronts marking the cold tongue, with variations on the order of 1–2 °C, periods of 20–40 days, wavelengths of 1000–2000 km, westward phase speeds around 0.5 m s^{-1} (Qiao and Weisberg, 1995; Contreras, 2002). Table 1 in Qiao and Weisberg (1995) compares historic references (dating from 1975 to 1990) that use varying types of data, many of which include estimates of zonal wavenumber and phase speed, to show these wave characteristics are averages. TIWs seem to be contained largely in the surface layer, with energy falling off sharply through the thermocline. However, a subsurface expression of these waves has been observed through energy propagation into the abyss (for references, see Qiao and Weisberg, 1995).

Since the cold tongue persists from July to November of each year, the TIWs are detectable in SST during the same time frame. By August, the waves are usually between 160° W and 100° W (Contreras, 2002), and by March the signal typically weakens. Interannually, TIWs are most energetic during La Niña years (Hashizume et al., 2001; Legeckis et al., 2004; Wang and Fiedler, 2006), and are weak or non-existent in the eastern equatorial Pacific during strong El Niño years, when the cold tongue signature, the SEC, and consequently the shear are weak. TIWs appear more prominent on the northern border of the cold tongue (Contreras,

2002), which ocean numerical models (Yu et al., 1995) suggest is due to the asymmetries of the two branches of the SEC and the equatorial SST front, and not due to the presence of the NECC.

The TIVs shape the equatorial upwelling into a succession of undulations of SST and chlorophyll fronts detected in remotely sensed data. In the Pacific, TIVs have a diameter of ~300–500 km, are found between latitudes 3° N to 8° N, and appear to form only north of the equator (Flament et al., 1996; Weidman et al., 1999; Legeckis et al., 2004). TIVs exhibit eddy currents exceeding 70 cm s^{-1}, a westward phase propagation speed of about 25–36 km d^{-1} (Weidman et al., 1999; Kennan and Flament, 2000), eastward energy propagation (Philander, 1976, 1978), and they depress the thermocline around 30 m at eddy center (Kennan and Flament, 2000). The cusps of the SST front seem to maintain a constant phase relationship with the TIVs (Weidman et al., 1999). Flament et al. (1996) and Kennan and Flament (2000) find that the cusps are due to northward advection on the leading edge of the TIVs of cold fresh water from the equatorial upwelling zone. In drifter data and shipboard ADCP measurements of a TIV, Kennan and Flament (2000) found (as expected) a depressed thermocline with a temperature signature observed to 180 m, recirculating saline water at depth, convergence along the perturbed North Equatorial Front, and upwelling near the TIV center. Kennan and Flament (2000) also found, from vortex entrainment, net equatorward heat of approximately 0.3×106 W m^{-2}. Weidman et al. (1999) found that dissipation occurred when they moved southward and seemed to run into the wave front.

Baturin and Niiler (1997) used Lagrangian drifters, equatorial moorings, radiometric SST maps, and ECMWF winds to study eddy kinetic and potential energy production in the TIW region. They maintain that TIWs reduced the shear of the mean current, in agreement with previous observations by Hansen and Paul (1984), and warmed the equatorial cold tongue by meridional advection (Swenson and Hansen, 1999; Kessler et al., 1998; Polito et al., 2001). The meridional heat advection across the equatorial Pacific is largest in the eastern Pacific (Wang and McPhaden, 1999), where it is dominated by the seasonally varying TIWs. Therefore, TIWs are key to understanding the heat balance in the region (Kessler, 2006; Wang and McPhaden, 1999).

3.4. Effects on ecosystems

TIVs seem to affect the marine ecosystem through reallocating nutrients, CO_2, primary productivity, phytoplankton, zooplankton, micronekton, and on up to the highest tropic levels (Pennington et al., 2006; Fernández-Alamo and Farber-Lorda, 2006). Here we summarize a study by Menkès et al. (2003) which used ship-based observations and satellite-derived SST and chlorophyll maps to describe the distribution of biological and chemical variables (e.g. nutrients, plankton and nekton) within a TIV in the Atlantic. They found that the upwelling near the vortex center (Flament et al., 1996; Kennan and Flament, 2000) does not appear to effect surface chlorophyll levels. The vortex advected cool, saline, nutrient-, chlorophyll- and zooplankton-rich water poleward and warm, fresher, nitrate-, chlorophyll-, zooplankton-poor waters equatorward. This transport enhanced primary production levels, extending to successively higher tropic levels farther northward, and increased the small pelagic fish concentration in the biologically enriched waters (Menkès et al., 2003).

3.5. Effects on the atmospheric boundary layer

Baturin and Niiler (1997) found air–sea interactions to be important to the total energy balance of the waves. The SST pattern of TIWs is reflected in the wind stress and Ekman pumping fields (Polito et al., 2001; Chelton et al., 2001). Polito et al. (2001) found their wind estimates and TIW surface measurements to be phase-locked. Hashizume et al. (2001) suggest in their study of the 1999 La Niña that SST-induced sea level pressure changes contributed substantially to wind fluctuations. TIW-induced SST anomalies were observed to affect temperatures throughout the whole depth of the atmospheric boundary layer (1–1.5 km deep) (Hashizume et al., 2002).

Chelton et al. (2001) support the hypothesis of Wallace et al. (1989) that the SST responds to the atmospheric boundary layer stabilization, and in turn, the surface winds vary in response to the SST. In slightly more detail (Chelton et al., 2001), the trade winds blow northwestward across the cold tongue, and the atmospheric boundary layer is stabilized by the cooler water. The stabilization decouples the surface winds

from the higher winds, decreasing the surface winds, and causing convergence of the surface wind stress. As the surface winds cross to warmer water north of the cold tongue, the atmospheric boundary layer is destabilized. The enhanced turbulent mixing of momentum from higher winds increases the surface winds, resulting in a divergence of the surface wind stress. Fig. 3 from Chelton et al. (2004) clearly shows a connection between SST fronts and both the wind stress curl and divergence fields in the eastern tropical Pacific. Their unfiltered fields show the wind patterns associated with the Equatorial Front much better than the spatial high-pass filtered fields, which show the wind jet patterns. Chelton et al. (2001) also found that the pressure gradient forcing (i.e. the SST influencing the surface winds) is a secondary dynamical mechanism when considering the impact on mesoscale ocean processes such as TIWs, but is more important on the larger scales.

4. Conclusions

Although many advances have been made in the understanding of the coastal eddies, and TIWs and TIVs in the eastern tropical Pacific, the main focus has been on the fundamental physical characteristics; therefore many specific physical aspects remain to be explained. More work has been done on the TIWs and associated TIVs than the coastal eddies; probably because they have basin-wide implications, and are observed in the Atlantic and the Pacific. For example, we know more about how the TIWs interact with, and are generated by general circulation, but we know little about how the coastal eddies affect, or are influenced by, general circulation (Kessler, 2006). The role of instability of the coastal currents in the generation of coastal eddies seems to be important and requires more study. Also, very little is known about the cyclonic coastal eddies. Although the interaction of these mesoscale phenomena with the atmospheric boundary layer has been well studied (Chelton et al., 2001, 2004; Amador et al., 2006), questions still remain about potential feedback on the smaller atmospheric scale between ocean and the atmosphere. Finally, the least studied aspect, regarding either the coastal eddies or the TIWs and TIVs, is their impact on the regional biogeochemical and ecosystem structure and dynamics, and this should be addressed by direct observation as well as by numerical modeling.

Acknowledgements

CSW wishes to thank P. Fiedler for offering the leadership in writing this review and W. Kessler for his encouragement and help in getting started. This is a contribution to the scientific agenda of the Eastern Pacific Consortium of the InterAmerican Institute for Global Change Research. RRL was supported by NASA contract 1221120. MFL's contribution is part of CONACYT (Mexico) projects G34601-S and D41881-F; he is currently at SIO-UCSD as recipient of a UCMEXUS-CONACYT sabbatical scholarship. Thanks to L. Zavala-Sanson for reviewing the manuscript, and to C. Cabrera and V. Godínez for technical support. Support was also provided by the Protected Resources Division of NOAA Fisheries, Southwest Fisheries Science Center.

References

Adem, J., 1956. A series solution for the barotropic vorticity equation and its application to the study of atmospheric vortices. Tellus 8, 364–372.

Amador, J.A., Alfaro, E.J., Lizano, O.G., Magaña, V.O., 2006. Atmospheric forcing of the eastern tropical Pacific: A review. Progress in Oceanography, 69 (2–4), 101–142.

Ballestero, D., Coen, J.E., 2004. Generation and propagation of anticyclonic rings in the Gulf of Papagayo. International Journal of Remote Sensing 25, 2217–2224.

Barton, E.D., Argote, M.L., Brown, J., Kosro, P.M., Lavín, M.F., Robles, J.M., Smith, R.M., Trasviña, A., Velez, H.S., 1993. Supersquirt: dynamics of the Gulf of Tehuantepec, Mexico. Oceanography 6, 23–30.

Baturin, N.G., Niiler, P.P., 1997. Effects of instability waves in the mixed layer of the equatorial Pacific. Journal of Geophysical Research – Oceans 102, 27771–27793.

Benestad, R.E., Sutton, R.T., Allen, M.R., Anderson, D.L.T., 2001. The influence of subseasonal wind variability on tropical instability waves in the Pacific. Geophysical Research Letters 28, 2041–2044.

Blackburn, M., 1962. An oceanographic study of the Gulf of Tehuantepec, US Fish and Wildlife Service, Special Scientific Report – Fisheries, 404, Washington DC.

Bourassa, M.A., Zamudio, L., O'Brien, J.J., 1999. Noninertial flow in NSCAT observations of Tehuantepec winds. Journal of Geophysical Research – Oceans 104, 11311–11319.

Brenes, C., Hernández, A., Gutiérrez, A., 1988. Sea surface thermohaline variations along the Nicaraguan Pacific coastal waters. Tópicos Meteorológicos y Oceanográficos 5, 17–25.

Caltabiano, A.C.V., Robinson, I.S., Pezzi, L.P., 2005. Multi-year observations of instability waves in the Tropical Atlantic Ocean. Ocean Science Discussions 2, 1–35.

Chelton, D.B., deSzoeke, R.A., Schlax, M.G., El Naggar, K., Siwertz, N., 1998. Geographical variability of the first-baroclinic Rossby radius of deformation. Journal of Physical Oceanography 28, 433–460.

Chelton, D.B., Freilich, M.H., Esbensen, S.K., 2000a. Satellite observations of the wind jets off the Pacific coast of Central America. Part I: Case studies and statistical characteristics. Monthly Weather Review 128, 1993–2018.

Chelton, D.B., Freilich, M.H., Esbensen, S.K., 2000b. Satellite observations of the wind jets off the Pacific coast of Central America. Part II: Regional relationships and dynamical considerations. Monthly Weather Review 128, 2019–2043.

Chelton, D.B., Esbensen, S.K., Schlax, M.G., Thum, N., Freilich, M.H., Wentz, F.J., Gentemann, C.L., McPhaden, M.J., Schopf, P.S., 2001. Observations of coupling between surface wind stress and sea surface temperature in the eastern tropical Pacific. Journal of Climate 14, 1479–1498.

Chelton, D.B., Schlax, M.G., Lyman, J.M., Johnson, G.C., 2003. Equatorially-trapped Rossby waves in the presence of meridionally-sheared baroclinic flow in the Pacific. Progress in Oceanography 56, 323–380.

Chelton, D.B., Schlax, M.G., Freilich, M.H., Milliff, R.F., 2004. Satellite measurements reveal persistent small-scale features in ocean winds. Science 303, 978–983.

Clarke, A.J., 1988. Inertial wind path and sea surface temperature patterns near the Gulf of Tehuantepec and the Gulf of Papagayo. Journal of Geophysical Research – Oceans 93, 15491–15501.

Crepon, M., Richez, C., 1982. Transient upwelling generated by two-dimensional atmospheric forcing and variability in the coastline. Journal of Physical Oceanography 12, 1437–1457.

Contreras, R.F., 2002. Long-term observations of tropical instability waves. Journal of Physical Oceanography 32, 2715–2722.

Cox, M.D., 1980. Generation and propagation of 30-day waves in a numerical model of the Pacific. Journal of Physical Oceanography 10, 1168–1186.

Cushman-Roisin, B., 1994. Introduction to Geophysical Fluid Dynamics. Prentice-Hall, Englewood Cliffs, NJ, 320 pp.

Cushman-Roisin, B., Chassignet, E.P., Tang, B., 1990. Westward motion of mesoscale eddies. Journal of Physical Oceanography 20, 758–768.

Duing, W., Hisard, P., Katz, E., Knauss, J., Meincke, J., Miller, L., Moroshkin, K., Philander, G., Rybnikov, A., Voigt, K., Weisberg, R., 1975. Meanders and long waves in the equatorial Atlantic. Nature 257, 280–284.

Enfield, D.B., Allen, J.S., 1983. The generation and propagation of sea level variability along the Pacific coast of Mexico. Journal of Physical Oceanography 13, 1012–1033.

Farber-Lorda, J., Lavín, M.F., Zapatero, M.A., Robles, J.M., 1994. Distribution and abundance of euphausiids in the Gulf of Tehuantepec during wind forcing. Deep-Sea Research 38, 359–367.

Farber-Lorda, J., Lavín, M.F., Guerrero-Ruiz, M.A., 2004. Effects of wind forcing on the trophic conditions, zooplankton biomass and krill biochemical composition in the Gulf of Tehuantepec. Deep-Sea Research II 51, 601–614.

Fernández-Alamo, M.A., Farber-Lorda, J., 2006. Zooplankton and the oceanography of the Eastern Tropical Pacific: A review. Progress in Oceanography, 69 (2–4), 318–359.

Fiedler, P.C., 2002. The annual cycle and biological effects of the Costa Rica Dome. Deep Sea Research I 49, 321–338.

Fiedler, P.C., Lavín, M.F., 2006. Introduction: A review of Eastern Tropical Pacific Oceanography. Progress in Oceanography, 69 (2–4), 94–100.

Fiedler, P.C., Talley, L.D., 2006. Hydrography of the eastern tropical Pacific: A Review. Progress in Oceanography, 69 (2–4), 143–180.

Firing, E., Beardsley, R.C., 1976. The behavior of a barotropic eddy on a Beta-plane. Journal of Physical Oceanography 6, 57–65.

Flament, P.J., Kennan, S.C., Knox, R.A., Niiler, P.P., Bernstein, R.L., 1996. The three dimensional structure of an upper ocean vortex in the tropical Pacific Ocean. Nature 383, 610–613.

Giese, B.S., Carton, J.A., Holl, L.J., 1994. Sea level variability in the eastern tropical Pacific as observed by TOPEX and the Tropical-Ocean Global Atmosphere Tropical-Atmosphere–Ocean Experiment. Journal of Geophysical Research – Oceans 99, 24739–24748.

Gonzalez-Silvera, A., Santamaría-de-Angel, E., Millán-Nuñez, R., Manzo-Monroy, H., 2004. Satellite observations of mesoscale eddies in the Gulfs of Tehuantepec and Papagayo (Eastern Tropical Pacific). Deep-Sea Research II 51, 587–600.

Hansen, D.V., Maul, G.A., 1991. Anticyclonic current rings in the eastern tropical Pacific Ocean. Journal of Geophysical Research – Oceans 96, 6965–6979.

Hansen, D.V., Paul, C.A., 1984. Genesis and effects of long waves in the equatorial Pacific. Journal of Geophysical Research – Oceans 89, 10431–10440.

Hurd, W.E., 1929. Northers of the Gulf of Tehuantepec. Monthly Weather Review 57, 192–194.

Hashizume, H., Xie, S.P., Liu, W.T., Takeuchi, K., 2001. Local and remote atmospheric response to tropical instability waves: A global view from space. Journal of Geophysical Research – Atmospheres 106, 10173–10185.

Hashizume, H., Xie, S.P., Fujiwara, M., Shiotani, M., Watanabe, T., Tanimoto, Y., Liu, W.T., Takeuchi, K., 2002. Direct observations of atmospheric boundary layer response to SST variations associated with tropical instability waves over the eastern equatorial Pacific. Journal of Climate 15, 3379–3393.

Jayne, S.R., Marotzke, J., 2002. The oceanic eddy heat transport. Journal of Physical Oceanography 32, 3328–3345.
Jochum, M., Malanotte-Rizzoli, P., Busalacchi, A., 2004. Tropical instability waves in the Atlantic Ocean. Ocean Modeling 7, 145–163.
Kennan, S.C., Flament, P., 2000. Observations of a tropical instability vortex. Journal of Physical Oceanography 30, 2277–2301.
Kessler, W.S., 2002. Mean three-dimensional circulation in the northeastern tropical Pacific. Journal of Physical Oceanography 32, 2457–2471.
Kessler, W.S., 2006. The circulation of the eastern tropical Pacific: A Review. Progress in Oceanography 69 (2–4), 181–217.
Kessler, W.S., McPhaden, M.J., 1995. Oceanic equatorial waves and the 1991–93 El Nino. Journal of Climate 8, 1757–1774.
Kessler, W.S., Rothstein, L.M., Chen, D.K., 1998. The annual cycle of SST in the eastern tropical Pacific, diagnosed in an ocean GCM. Journal of Climate 11, 777–799.
Lawrence, S.P., Angell, J.P., 2000. Evidence for Rossby wave control of tropical instability waves in the Pacific Ocean. Geophysical Research Letters 27, 2257–2260.
Legeckis, R.V., 1977. Long waves in the eastern equatorial ocean. Science 197, 1177–1181.
Legeckis, R.V., Pichel, W., Nesterczuk, G., 1983. Equatorial long waves in geostationary satellite observations and in a multichannel sea surface temperature analysis. Bulletin of the American Meteorological Society 6 (2), 133–139.
Legeckis, R., Brown, C.W., Bonjean, F., Johnson, E.S., 2004. The influence of tropical instability waves on phytoplankton blooms in the wake of the Marquesas Islands during 1998 and on the currents observed during the drift of the Kon-Tiki in 1947. Geophysical Research Letters 31, L23307.
Martinez-Diaz-de-Leon, A., Robinson, I.S., Ballestero, D., Coen, E., 1999. Wind driven ocean circulation features in the Gulf of Tehuantepec, Mexico, revealed by combined SAR and SST satellite sensor data. International Journal of Remote Sensing 20, 1661–1668.
Masina, S., Philander, S.G.H., Bush, A.B.G., 1999. An analysis of tropical instability waves in a numerical model of the Pacific Ocean. 2. Generation and energetics of the waves. Journal of Geophysical Research – Oceans 104, 29637–29661.
Matsuura, T., Yamagata, T., 1982. On the evolution of nonlinear planetary eddies larger than the radius of deformation. Journal of Physical Oceanography 12, 440–456.
McClain, C.R., Christian, J.R., Signorini, S.R., Lewis, M.R., Asanuma, I., Turk, D., Dupouy-Douchement, C., 2002. Satellite ocean-color observations of the tropical Pacific Ocean. Deep-Sea Research II 49, 2533–2560.
Menkès, C., Kennan, S.C., Flament, P., Dandonneau, Y., Marchal, E., Biessy, B., Eldin, G., Masson, S., Lebourges, A., Moulin, C., Champalbert, G., Grelet, J., Montel, Y., Herbland, A., Morlière, A., 2003. A whirling ecosystem in the equatorial Atlantic. Geophysical Research Letters 29. doi:10.1029/2001GL014576.
McCreary, J.P., Lee, H.S., Enfield, D.B., 1989. The response of the coastal ocean to strong offshore winds: with application to circulations in the Gulf of Tehuantepec and Papagayo. Journal of Marine Research 47, 81–109.
Müller-Karger, F.E., Fuentes-Yaco, C., 2000. Characteristics of wind-generated rings in the eastern tropical Pacific Ocean. Journal of Geophysical Research – Oceans 105, 1271–1284.
Nof, D., 1983. On the migration of isolated eddies with application to Gulf Stream rings. Journal of Marine Research 41, 399–425.
Pennington, J.T., Mahoney, K.L., Kuwahara, V.S., Kolber, D.D., Calienes, R., Chavez, F.P., 2006. Primary production in the eastern tropical Pacific: a review. Progress in Oceanography 69 (2–4), 285–317.
Philander, S.G.H., 1976. Instabilities of zonal equatorial currents. Journal of Geophysical Research – Oceans 81, 3725–3735.
Philander, S.G.H., 1978. Instabilities of zonal equatorial currents, 2. Journal of Geophysical Research – Oceans 83, 3679–3682.
Polito, P.S., Ryan, J.P., Liu, W.T., Chavez, F.P., 2001. Oceanic and atmospheric anomalies of tropical instability waves. Geophysical Research Letters 28, 2233–2236.
Qiao, L., Weisberg, R.H., 1995. Tropical instability wave kinematics: Observations from the Tropical Instability Wave Experiment. Journal of Geophysical Research – Oceans 100, 8677–8693.
Qiao, L., Weisberg, R.H., 1998. Tropical instability wave energetics: Observations from the Tropical Instability Wave Experiment. Journal of Physical Oceanography 28, 345–360.
Robles-Jarero, E.G., Lara-Lara, J.R., 1993. Phytoplankton productivity in the Gulf of Tehuantepec. Journal of Plankton Research 15, 1341–1358.
Roden, G.I., 1961. On the wind-driven circulation in the Gulf of Tehuantepec and its effect upon surface temperatures. Geofisica Internacional 1, 55–72.
Romero-Centeno, R., Zavala-Hidalgo, J., Gallegos, A., O'Brien, J.J., 2003. Isthmus of Tehuantepec wind climatology and ENSO signal. Journal of Climate 16, 2628–2639.
Samuelsen, A., 2005. Modeling the effect of eddies and advection on the lower trophic ecosystem in the northeast tropical Pacific. Ph.D. Thesis, Florida State University, 86 pp.
Spillane, M.C., Enfield, D.B., Allen, J., 1987. Intraseasonal oscillations in sea level along the west coast of the Americas. Journal of Physical Oceanography 17, 313–325.
Steenburgh, W.J., Schultz, D.M., Colle, B.A., 1998. The structure and evolution of gap otflow over the Gulf of Tehuantepec, Mexico. Monthly Weather Review 126, 2673–2691.
Stumpf, H.G., 1975. Satellite detection of upwelling in the Gulf of Tehuantepec, Mexico. Journal of Physical Oceanography 5, 383–388.
Stumpf, H.G., Legeckis, R.V., 1977. Satellite observations of mesoscale eddy dynamics in the eastern tropical Pacific Ocean. Journal of Physical Oceanography 7, 648–658.
Swenson, M.S., Hansen, D.V., 1999. Tropical Pacific ocean mixed layer heat: The Pacific cold tongue. Journal of Physical Oceanography 29, 69–81.
Thomas, L.N., Rhines, P.B., 2002. Nonlinear stratified spin-up. Journal of Fluid Mechanics 473, 211–244.

Trasviña, A., Barton, E.D., Brown, J., Velez, H.S., Kosro, P.M., Smith, R.L., 1995. Offshore wind forcing in the Gulf of Tehuantepec, Mexico: the asymmetric circulation. Journal of Geophysical Research – Oceans 100, 20649–20663.

Trasviña, A., Barton, E.D., Velez, H.S., Brown, J., 2003. Frontal subduction of a cool surface water mass in the Gulf of Tehuantepec, Mexico. Geofísica Internacional 42, 101–114.

Umatani, S., Yamagata, T., 1991. Response of the eastern tropical Pacific to meridional migration of the ITCZ: the generation of the Costa Rica Dome. Journal of Physical Oceanography 21, 346–363.

Wang, W.M., McPhaden, M.J., 1999. The surface-layer heat balance in the equatorial Pacific Ocean. Part I: Mean seasonal cycle. Journal of Physical Oceanography 29, 1812–1831.

Wang, C., Fiedler, P.C., 2006. ENSO variability in the eastern tropical Pacific: A review. Progress in Oceanography 69 (2–4), 239–266.

Wallace, J.M., Mitchell, T.P., Deser, C., 1989. The influence of sea surface temperature on surface wind in the eastern equatorial Pacific: Seasonal and interannual variability. Journal of Climate 2, 1492–1499.

Weidman, P.D., Mickler, D.L., Dayyani, B., Born, G.H., 1999. Analysis of Legeckis eddies in the near-equatorial Pacific. Journal of Geophysical Research – Oceans 104, 7865–7887.

Willett, C.S., 1996. A study of anticyclonic eddies in the eastern tropical Pacific Ocean with integrated satellite, in situ, and modelled data. Ph.D. thesis, University of Colorado, Boulder, Colorado.

Yu, J.Y., Liu, W.T., 2003. A linear relationship between ENSO intensity and tropical instability wave activity in the eastern Pacific Ocean. Geophysical Research Letters 30, 1735.

Yu, Z., McCreary, J.P., Proehl, J.A., 1995. Meridional asymmetry and energetics of tropical instability waves. Journal of Physical Oceanography 25, 2997–3007.

Zamudio, L., Leonardi, A.P., Meyers, S.D., O'Brien, J.J., 2001. ENSO and eddies on the southwest coast of Mexico. Geophysical Research Letters 28, 13–16.